Electron Paramagnetic Resonance Line Shifts and Line Shape Changes Due to Spin Exchange of Nitroxide Free Radicals in Liquids. 7. Singly Charged Surfactant Nitroxide

Barney L. Bales,*,‡ Francis L. Harris,† Mirna Peric,‡ and Miroslav Peric‡

Department of Chemistry and Department of Physics and Astronomy and The Center for Supramolecular Studies, California State University at Northridge, Northridge, California 91330

Received: June 6, 2009; Revised Manuscript Received: June 27, 2009

EPR spectra of aqueous solutions of the singly charged surfactant nitroxide 4-[*N*,*N*-dimethyl-*N*-(*n*-dodecyl)ammonium]-2,2,6,6-tetramethylpiperidinyl-*N*-oxy bromide-d_{16} (DCAT12) are studied as functions of the molar concentration, $c = 0.1-8$ mM, and the temperature from 273 to 353 K. This concentration range is below the critical micelle concentration, cmc, at which DCAT12 forms micelles. Spin−spin broadening of the EPR lines averaged over the three lines is separated into contributions due to spin exchange, $\langle B_e \rangle$, and dipolar, $\langle B_{dip} \rangle$, interactions yielding values of the fractional broadening by spin exchange, $\Omega(T)$, that vary from near unity at 353 K to approximately 50% at 273 K. This compares with a variation from unity to approximately 77% for a neutral spin probe perdeuterated 2,2,6,6-tetramethyl-4-oxopiperidine-1-oxyl (PDT) over the same range. Unlike PDT and the Stokes−Einstein prediction, the broadening constant by spin exchange, $d\langle B_e \rangle/dc$, is not linear with T/η, where η is the shear viscosity, instead following a quadratic dependence. Nevertheless, $d\langle B_e \rangle/dc$ is remarkably close to a hydrodynamic prediction using the Stokes−Einstein equation modified to take the spin probe charge into account. Compared with PDT, values of $d\langle B_e \rangle/dc$ are decreased and $d\langle B_{dip} \rangle/dc$ increased at all temperatures, while the values of the re-encounter rate, τ_{RE}^{-1}, deduced from line shifts, are reduced. Interestingly, values of $d\langle B_{dip} \rangle/dc$, $\Omega(T)$, and τ_{RE}^{-1} are comparable for PDT and DCAT12 when compared at the same rotational diffusion rates.

Introduction

Spin exchange between nitroxide spin probes is becoming a rich source of detailed information about molecular collisions in liquids.[1−8] Spin exchange broadens and shifts the EPR lines while introducing a spin-exchange induced dispersion into the spectra.[1−8] The broadening is a sum of the contributions from spin exchange, B_e, and dipolar interactions, B_{dip}. The broadening due to spin exchange alone may be deduced from the spin exchange induced dispersion that may be subtracted from the total broadening to give the broadening by dipolar interactions. The spin exchange frequency, ω_e, may be calculated from the broadening by spin exchange. The line shifts have turned out to be richer in content than previously thought, being composed of two components, one varying linearly and the other quadratically with ω_e. The quadratic term yields an independent measure of ω_e. We model nitroxide−nitroxide collisions as first-time collisions, referred to as encounters, followed by a series of re-encounters prior to the diffusing pair's escaping each other's presence. The mean time between re-encounter collisions is denoted by τ_{RE}.

Particularly interesting was the discovery[2] that re-encounter collisions can introduce a component into the line shifts that is linear in ω_e for cases in which the spin exchange interaction is strong, i.e., $|J\tau_c| \gg 1$ where J and τ_c are the minus two times the exchange integral and the duration of the collision, respectively. We recently proposed that the experimentally observed linear term was indeed due to re-encounter collisions[5] and have provided support from experiments involving both ^{14}N and ^{15}N nitroxides.[6] Provided that this proves to be true after further testing, the linear term offers exciting insight into the behavior of two nitroxides while they are in close proximity colliding with one another within a solvent "cage".

TABLE 1: Fit Parameters for Each Line of an EPR First-Derivative Spectrum[a]

parameter	description
$V_{disp}(c)_{M_I}$	maximum height of dispersion[b]
$V_{pp}(c)_{M_I}$	peak-to-peak height of absorption
$\Delta H^0_{pp}(c)_{M_I}$	peak-to-peak overall line width
$H(M_I)$	resonance field of absorption[c]
$\eta(M_I)$	Gaussian−Lorentzian mixing parameter

[a] $M_I = +1$, 0, and -1 label the hyperfine lines from low- to high-field. [b] Positive if above the baseline in conventional presentation with the doubly integrated intensity positive. [c] Not the field where the spectrum crosses the baseline in the presence of dispersion.

To summarize recent progress, we are able to independently measure the effects of (1) spin exchange interactions, (2) dipolar interactions, and (3) re-encounter collision rates at a single temperature with good precision. This work was motivated by asking what happens to these effects if the nitroxides are charged. There is some theoretical insight into the effect on spin exchange due to the work of Debye,[9] but, to our knowledge, nothing is known on the other two. The reader might find it interesting to predict the qualitative effect of a charge on dipolar interactions and re-encounter collision rates.

In this work, we begin a series of studies of nitroxides bearing a single charge. In our first effort, we study the surfactant nitroxide 4-[*N*,*N*-dimethyl-*N*-(*n*-dodecyl)ammonium]-2,2,6,6-tetramethylpiperidinyl-*N*-oxy bromide-d_{16} (DCAT12) because above the critical micelle concentration (cmc) the presence of micelles[10,11] presents an interesting system for those interested in both micelles and molecular collisions in liquids. Protons

* Corresponding author. E-mail: barney.bales@csun.edu. Webpage: http://www.csun.edu/~vcphy00s/BBVita.html.
† Department of Chemistry.
‡ Department of Physics and Astronomy and The Center for Supramolecular Studies.

10.1021/jp905335r CCC: $40.75
Published on Web 07/29/2009

TABLE 2: Quantities Computed from Least-Squares Fit Parameters for ^{14}N Nitroxides (List of First 11 Equations)

parameter[a]		description
$\Delta H_{pp}^{L}(M_I)$		intrinsic (Lorentzian) line width[b]
$\Delta H_{pp}^{G}(M_I)$		Gaussian line width[c]
$A_{universal}(M_I)$	(1)[d]	doubly integrated intensity
$c(\mathrm{EPR}) = \mathrm{Factor} \cdot \langle A_{univsersal} \rangle$	(2)	estimate of concentration from $A_{universal}(M_I)$, averaged over M_I where "Factor" is determined from fresh samples of PDT; see text
$\chi(M_I) = \Delta H_{pp}^{G}(M_I)/\Delta H_{pp}^{L}(M_I)$		inhomogeneous broadening parameter
$B_{tot}(M_I) = \Delta H_{pp}^{L}(c)_{M_I} - \Delta H_{pp}^{L}(0)_{M_I}$	(3)	total broadening
$\langle B_{tot} \rangle = \frac{1}{3}[B_{tot}(+) + B_{tot}(0) + B_{tot}(-)]$	(4)	average total broadening; $\langle B_e \rangle$ and $\langle B_{dip} \rangle$ similarly defined
$\left[\frac{V_{disp}}{V_{pp}}\right]_{\pm} = V_{disp}(\pm)/V_{pp}(\pm) - V_{disp}(0)/V_{pp}(0)$	(5)	dispersion-absorption ratios corrected for instrument dispersion
$\left[\frac{V_{disp}}{V_{pp}}\right]_{\pm}^{\#} = \left[\frac{V_{disp}}{V_{pp}}\right]_{\pm}\left[1 - 0.707\left[\frac{V_{disp}}{V_{pp}}\right]_{\pm}^{2}\right]$	(6)	dispersion corrected to vary linearly with $\langle B_e \rangle/A_0$
$A_{abs} = \frac{1}{2}[H(-) - H(+)]$	(7)	$A_{abs} \rightarrow A_0$ in the limit $c \rightarrow 0$
τ_B, τ_C	(8)[e]	rotational correlation times; $\tau_{rot} = (\tau_B \tau_C)^{1/2}$
$\Omega(T)_{\pm} = \frac{\mathrm{d}\left[\frac{V_{disp}}{V_{pp}}\right]_{\pm}^{\#}}{\mathrm{d}\langle B_{tot}/A_0 \rangle}$	(9)	fractional broadening by spin exchange; derivative evaluated from linear portion of the $[V_{disp}/V_{pp}]_{\pm}^{\#}$ versus $\langle B_{tot}/A_0 \rangle$ curves
$B_e(M_I) = B_{tot}(M_I) \cdot \Omega(T)$	(10)	spin exchange broadening
$B_{dip}(M_I) = B_{tot}(M_I) - B_e(M_I)$	(11)	dipolar broadening

[a] The dependence on c is suppressed unless expressly needed. [b] Equation 7b of ref 21. [c] Equation 7c of ref 21. [d] Equations 18 and 34 of ref 21. [e] Equations 29 and 30 of ref 32.

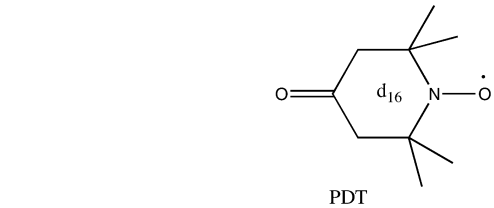

PDT

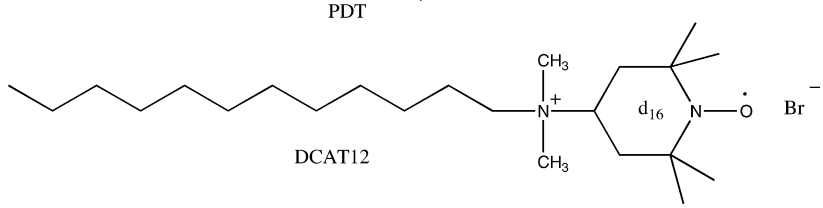

DCAT12

are replaced by deuterons at all positions in the ring except at the attachment point of the tail. Nitroxides similar to DCAT12, although not deuterated, have found use in biological studies.[12−16]

In this work, we restrict our attention to concentrations below the cmc and compare the results with those taken from the literature for a neutral nitroxide perdeuterated 2,2,6,6-tetramethyl-4-oxopiperidine-1-oxyl (PDT). There is no experimental information in the literature about the effect of a charge on re-encounter frequencies or the importance of dipolar versus spin exchange interactions. We were particularly curious about the effect of a single charge on the rate of re-encounter collisions, τ_{RE}^{-1}, because the doubly charged peroxylamine disulfonate (Fremy's salt) is the only case found so far in which the line shifts are well described by the quadratic term only. We suggested two possibilities: (1) re-encounters are prevented by the electrostatic repulsion of the doubly charged molecules or (2) strong spin exchange does not prevail.[7] We planned this work thinking that we would gain insight into these possibilities; however, we find that strong spin exchange does prevail and τ_{RE}^{-1} is even faster than predicted by hydrodynamic theory provided that the charge is taken into account. Thus, we still do not know if either (1) or (2) explains the results in Fremy's salt.

The only published work on spin−spin interactions of singly charged nitroxides was by Martini and Bindi[17] who measured the concentration broadening of the sodium salt of 2,2,5,5-tetramethylprrrolidin-1-oxyl-3-carboxolate in water as a function of temperature. Those authors claim to separate the effects of dipolar and spin exchange interactions; however, unfortunately, the spectra were incorrectly analyzed because inhomogeneous broadening due to unresolved hyperfine structure was not properly treated. Furthermore, Martini and Bindi[17] measured only the line widths, from which reliable separation of the two interactions cannot be obtained.[7]

Eastman et al.[18] have discussed the qualitative features of the behavior of exchange broadening on the basis of standard Debye theory[9,19] which breaks down at rather low concentrations. Others[20] have tried to construct empirical descriptions of spin exchange between paramagnetic ions and spin probes.

Unfortunately, the field is at an awkward moment in which we are able to study molecular collisions in liquids in more detail than we can describe them theoretically: thus, the present paper offers a modest beginning to seek a better understanding of the collision process from the experimental side, hopefully offering some insights that will be useful in formulating better empirical understanding.

Theory

The theory has been presented in detail in this series and references therein,[1−8] which may be consulted for a detailed, conventional presentation. Here, we summarize the theory associated with the analysis of the EPR spectra in Tables 1 and 2. All EPR spectral lines are least-squares fit to a model of the sum of the contributions by a Voigt absorption and Lorentzian dispersion. The quantities resulting from the fits are summarized in Table 1, and Table 2 summarizes eqs 1−11. The mixing parameter $\eta(M_I)$ permits the separation of the homogeneous and inhomogeneous contributions to the observed line width and is used to correct the parameters that are affected by the inhomogeneous contribution.[21]

Hydrodynamic estimates of the quantities of interest in this work are available[22] employing the Stokes−Einstein equation as follows:

$$\frac{\mathrm{d}}{\mathrm{d}c}\langle B_e\rangle^{SE} = f_e^* C_e \frac{T}{\eta}\frac{r_{ex}}{a} \tag{12}$$

where η is the shear viscosity, a is the hydrodynamic radius controlling the translational diffusion, and $2r_{ex}$ is the distance between the two nitroxides where spin exchange is effective. In eq 12, f_e^* is a factor that is unity for neutral nitroxides and takes into account electrostatic interactions between charged particles. In 1942, Debye[9] derived an expression for f_e^* valid in the limit of small concentration. For singly charged particles of the same charge sign, in the absence of added electrolyte, $f_e^* = 0.45$; see, for example p 538 of ref 23. We call eq 12 with $f_e^* = 0.45$, the hydrodynamic dilute (HD) limit. In the presence of added electrolyte, Eastman et al.[18] have approximated f_e^* but point out that the results are qualitative. Note that the commonly quoted second-order spin exchange rate constant[1] may be computed as follows: $K_e = (3(3^{1/2})\gamma/4)(\mathrm{d}\langle B_e\rangle/\mathrm{d}c)$.

The hydrodynamic prediction for the dipolar broadening constant is given by

$$\frac{\mathrm{d}}{\mathrm{d}c}\langle B_{dip}\rangle^{SE} = \frac{1}{f_{dip}^*} C_{dip}\frac{\eta}{T}\frac{a}{r_c} \tag{13}$$

where $2r_c$ is the distance of closest approach between the two spin dipoles.[22] The factor f_{dip}^* is equal to unity for uncharged nitroxides; however, to our knowledge, it is unknown for charged particles.

For nitroxides, $C_e = 0.485$ (cP·G)/(M·deg) and $C_{dip} = 763$ (deg·G)/(cP·M). In the limit $T/\eta = 0$, $\mathrm{d}\langle B_{dip}\rangle/\mathrm{d}c = C_{dip}^{static} = 49.03$ G/M.[22]

The Stokes−Einstein prediction for the mean time between re-encounters[2] is given by

$$\tau_{RE} = \frac{1}{f^*_{RE}} \frac{3\pi b^3 \eta}{2kT} \quad (14)$$

where b is the distance between the spin probes at collision. The factor f^*_{RE} is equal to unity for uncharged nitroxides. One might think that $f^*_{RE} = f^*_e$ because both re-encounters and encounters involve the collision of the two spin probes; nevertheless, a moment's thought about Debye's derivation[9] of the HD brings into doubt this assumption. Debye followed Smoluchowski's[24] original approach and calculated the probability that two charged particles will collide under the influence of a screened electrostatic potential. The existence of a diffuse ionic cloud reduces the long-range electrostatic potential leading to $f^*_e = 0.45$ in the HD limit; however, it is not obvious how or if the cloud would intervene between two nitroxides while diffusing in close proximity within a cage. Without the influence of the diffuse cloud, one might expect f^*_{RE} to be even less than 0.45.

Similarly, hydrodynamic estimates for rotational correlation times[25] are available from the Stokes−Einstein−Debye equation yielding

$$\tau_{rot} = \frac{4\pi}{3} a^3 \cdot \frac{\eta}{kT} \quad (15)$$

where we have tacitly assumed that the hydrodynamic radius for translation is the same as for rotation.

The broadening constants $d\langle B_e\rangle/dc$ and $d\langle B_{dip}\rangle/dc$ are rather independent of the probe size because a, r_c, and r_e must be very similar.[1,22] The rate τ_{RE}^{-1} *does* depend on the distance of closest approach b. Employing the reasonable assumption that this distance is equal to the diameter of the probes, $2a = b$, we may determine a from eq 15 and use it to compute hydrodynamic predictions of the values of τ_{RE}^{-1}.

Employing the assumption $b = 2a$ and combining eqs 14 and 15, we arrive at the very simple universal prediction

$$\tau_{rot}^{-1} = \frac{9}{f^*_{RE}} \tau_{RE}^{-1} \quad (16)$$

For uncharged molecules, the rotational rate is predicted to be 9 times that of the re-encounter rate independent of size, temperature, or viscosity, a result that ought to be straightforward to test.

Experimental values of τ_{RE}^{-1} are found by fitting values of A_{abs}/A_0 by varying the parameter κ in eq 17:[6]

$$\frac{A_{abs}}{A_0} = 1 - \kappa \frac{B_e}{A_0} - \frac{9}{32}\left(\frac{B_e}{A_0}\right)^2 \quad (17)$$

and from the resulting values of κ, values of the re-encounter time, τ_{RE}, are computed using[2]

$$\kappa = \frac{\sqrt{3}}{8}(1 + \sqrt{2})\sqrt{\gamma A_0 \tau_{RE}/2} \quad (18)$$

where γ is the gyromagnetic ratio of the electron. The determination of τ_{RE} becomes more difficult as dipolar interactions become more significant because of the error in separating B_e from B_{tot}.

SCHEME 1: DCAT12 Synthesis

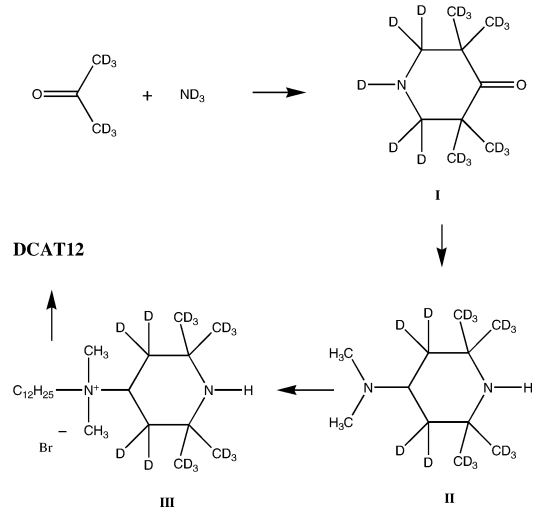

Experimental Section

1,3,3,5,5-Pentadeuterio-2,2,6,6-tetrakis(trideuteriomethyl)piperidin-4-one (I) (Scheme 1). Liquid trideuterioammonia (1.2 mL, 1.0 g) was allowed to vaporize into a vigorously stirred suspension of powdered anhydrous calcium chloride (3 g) in hexadeuterioacetone (10 g) at room temperature. The suspension was then stirred for 4 days. The orange reaction mixture was cooled in ice and quenched by slow addition of 5 mL of a solution of approximately 40% KOD in deuterium oxide with vigorous stirring. The supernatant was decanted and the yellow paste residue was extracted repeatedly with diethyl ether. The combined organic layer was dried over magnesium sulfate and the solvent was removed at reduced pressure to leave an orange residue (1.67 g) that crystallized when chilled. The sample was purified by flash chromatography on silica with diethyl ether eluent to provide 970 mg of a light orange oil which crystallized as long needles. This material was used without further purification.

4-(Dimethylamino)-3,3,5,5-tetradeuterio-2,2,6,6-tetrakis(trideuteriomethyl)piperidine (II) (Scheme 1). To a solution of dimethylamine hydrochloride (2.26 g, 21.7 mmol, 5 equiv) in methanol-*O-d* (5 mL) was added KOD (0.47 g), and the mixture was stirred until the base dissolved and KCl precipitated. **I** (953 mg, 5.54 mmol) in methanol-*O-d* (2.5 mL) was added and the suspension was heated at 50 °C for 45 min. Then a solution of sodium cyanoborohydride (1.74 g, 5 eq "borane") was added in methanol-*O-d* solution (5 mL) over 45 min. The reaction mixture was then stirred for an additional hour at 50 °C and then cooled. KOH (4 g) was added, and the suspension was stirred until the pellets dissolved. The mixture was filtered by suction, and the salts were washed with diethyl ether. The methanol layer was concentrated and extracted with diethyl ether. The combined ether solution was washed twice with a small amount of brine and dried over potassium carbonate. Solvent was removed at reduced pressure at no higher than 45 °C to leave an orange oil (972 mg, 88% crude yield). This material was purified by flash chromatography on silica, first with diethyl ether to eliminate a yellow impurity and then with 1% butylamine in diethyl ether to elute the major component as a yellow oil, 868 mg. This was further purified by Kugelrohr distillation (60 deg, 0.1 mm) to provide a colorless oil, 659 mg (59%).

4-*n*-Dodecyldimethylammonium-3,3,5,5-tetradeuterio-2,2,6,6-tetrakis(trideuteriomethyl)piperidine Bromide (III) (Scheme 1). The tertiary amine **II** (471 mg, 2.36 mmol) and *n*-bromododecane (0.65 mL, 676 mg, 1.15 eq, 2.71 mmol) were

TABLE 3: EPR Parameters at $c \rightarrow 0$ for DCAT12

T, K	A_0, G[a]	$\langle \Delta H_{pp}^G \rangle$, G[b]	$\langle \Delta H_{pp}^G \rangle_{MA=0}$, G[c]	$\tau_{rot} = [\tau_B \tau_C]^{1/2}$, ns[a]	τ_B/τ_C[a]
273	16.841 ± 0.001	0.753 ± 0.005	0.564	0.228 ± 0.001	1.04 ± 0.003
283	16.815 ± 0.002	0.746 ± 0.013	0.554	0.141 ± 0.001	0.990 ± 0.029
298	16.768 ± 0.002	0.741 ± 0.002	0.546	0.0774 ± 0.0002	0.991 ± 0.003
313	16.722 ± 0.001	0.734 ± 0.002	0.538	0.0511 ± 0.0002	1.09 ± 0.006
333	16.656 ± 0.001	0.732 ± 0.003	0.535	0.0313 ± 0.0003	1.18 ± 0.037
353	16.578 ± 0.001	0.723 ± 0.002	0.523	0.0204 ± 0.0002	1.31 ± 0.018

[a] Mean value and standard deviation of five spectra. [b] Mean value and standard deviation all three lines of five spectra. [c] Corrected for 1-G modulation amplitude (MA) to intrinsic values.[33]

heated together under a nitrogen atmosphere for 43 h at 80 °C. The product after cooling was an orange glass that flaked upon grinding with a spatula. This was triturated several times with petroleum ether (30−60 °C); the first-formed sticky ball became a tractable solid after the third wash. This was dried with a pump to leave an off-white powder, 933 mg, 78% yield. This material was used without further purification.

DCAT12 (Scheme 1). Compound III (933 mg, 2.08 mmol) was dissolved in methanol (5 mL) and the solution was added to a solution of sodium tungstate dihydrate (65 mg) and tetrasodium EDTAate trihydrate in water (4 mL). This mixture deposited some salts. Hydrogen peroxide (30%, 0.75 mL) was added dropwise, and the cloudy mixture was stirred at room temperature for 3 days. Small portions of sodium tungstate dihydrate and tetrasodium EDTAate trihydrate were added, followed by methanol (2 mL) and hydrogen peroxide (30%, 0.3 mL), and the orange nonhomogeneous mixture was heated in an oil bath at 35 °C. After 1 more day, the mixture was cooled to room temperature and more hydrogen peroxide (30%, 0.3 mL) was added. After each of the following 2 days, further portions of sodium tungstate dihydrate, tetrasodium EDTAate trihydrate, and hydrogen peroxide (as just previously) were added and stirring was continued at room temperature. After a total of 10 days, the mixture was extracted with dichloromethane (2 × 20 mL). This extract was dried over magnesium sulfate, and solvent was removed at reduced pressure to leave reddish-orange thick oil, 808 mg, which began to solidify upon standing. This was triturated twice with petroleum ether (30−60 °C) with centrifugation to provide an orange, soapy solid. Three crystallizations from a mixture of petroleum ether (30−60) and dichloromethane provided the desired cationic nitroxide, 60 mg. The mother liquors were combined and another crop of crystals was collected by a similar procedure, 90 mg.

Sample Preparation and EPR Measurements. A stock solution of 37 mM DCAT12 was prepared in Milli-Q water by weight and diluted by weight to form a series of molar concentrations c. EPR affords a convenient measure of radical concentrations, c(EPR), because they are proportional to the doubly integrated spectral intensity. For DCAT12, values of c(EPR) were computed using eq 2 (Table 2). "Factor" in eq 2, which depends on the temperature, was determined using freshly prepared aqueous solutions of PDT employing the same sample preparation, placement, and experimental conditions. For DCAT12, averaged over $c = 2-8$ mM, $c(\text{EPR}) = 0.95 \pm 0.02c$. Curiously, for $c = 0.1$ mM, $c(\text{EPR}) = 0.89 \pm 0.01c$, thus there is a loss in detected signal of the surfactant nitroxide at low concentrations. The accuracy of c(EPR) is estimated to be ±2%; the relative concentrations are accurate to ±1%. Undegassed samples were sealed into 50 μL pipets and placed into sample tubes housed in Bruker's nitrogen gas-flow temperature control dewar. The temperature, accurate to ±1 K, was measured with a thermocouple placed just above the active portion of the microwave cavity. During each spectrum, the temperature was stable to ±0.1 K. Five EPR spectra were acquired, one after the other, with a Bruker 300 ESP X-band spectrometer interfaced with Bruker's computer employing a sweep time of 41 s; time constant, 10 ms; microwave power, 5 mW; and sweep width, 70 G. The modulation amplitude was set at 1.0 G, comparable to the minimum observed total line widths. This improves the signal-to-noise ratio of low concentration spectra and broadens the Gaussian component of the lines by the difference in columns 3 and 4 of Table 3, leaving the Lorentzian component unchanged. The magnetic field sweep width was measured with Bruker's NMR Gaussmeter operating in the 1 mG resolution mode and was averaged over a day's run.

Results

EPR spectra of DCAT12 at concentrations below the cmc are similar to those published in recent papers.[3,4,7,8] Fits of Gaussian−Lorentzian sum functions to these spectra yielded parameters summarized in Table 1 and were analyzed to give the quantities in Table 2. The results in the limit $c \rightarrow 0$, where dipolar and spin exchange interactions are negligible, are tabulated in Table 3.

At low concentrations and temperatures, the ratio of the inhomogeneous to the intrinsic line width, $\chi = \Delta H_{pp}^G/\Delta H_{pp}^L$, reaches values in excess of 3. Thus, even though this probe is deuterated, reducing significantly the effect of unresolved hyperfine structure, it is critical to correct for inhomogeneous broadening to obtain accurate values of the intrinsic line width, ΔH_{pp}^L, from which the broadening is calculated. For example, at 298 K, the overall line width, $\Delta H_{pp}^0 = 0.865 \pm 0.001$ G and $\Delta H_{pp}^L = 0.237 \pm 0.002$ G; thus, ignoring the correction leads to an error of 265%, and this percentage is a strong function of both temperature and concentration, so even the relative values of the broadening are not valid when computed from ΔH_{pp}^0.

The cmc of CAT12 (not deuterated) was measured by Fox using conductivity with the following results: 8.7 ± 0.02, 9.3 ± 0.02, and 9.1 ± 0.02 mM at 298, 313, and 333 K, respectively.[11] Except for Figures 1−3 all of the results in this paper are derived from c(EPR) ≤ 8 mM, thus pertaining to spin−spin interactions in the absence of micelles. Figure 1 gives spectra of DCAT12 well above the cmc at three temperatures, showing the presence of the micelle line as a broad, underlying single line. The least-squares fits to the three narrow monomer lines and the micelle line are given in Figure 2. The smaller trace in each case in Figure 1 is the difference in the experimental spectrum and the fits. The three monomer lines and the micelle line in Figure 2 are sums of absorption and dispersion lines of Voigt shape. To save space, we have not presented separate traces of the absorption and dispersion components; examples of these separated traces may be found in Figure 1 of ref 8.

Figure 3 shows values of c(EPR) for DCAT12 derived from fits of the narrow lines versus c. The cmc = 8.0 ± 0.5 mM is

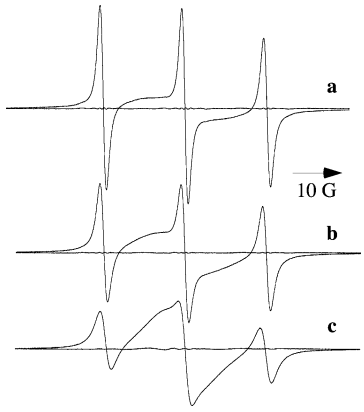

Figure 1. EPR spectra of 37-mM DCAT12 in water at (a) 298 K, (b) 313 K, and (c) 333 K. The smaller traces near the baselines are the differences in the observed spectra and the least-squares fits that are presented in Figure 2. The doubly integrated intensity of the micelle line is constant within ±0.7%. As the temperature increases, the line width of the micelle line decreases while those of the monomer increase, accounting for the increasing prominence of the micelle line.

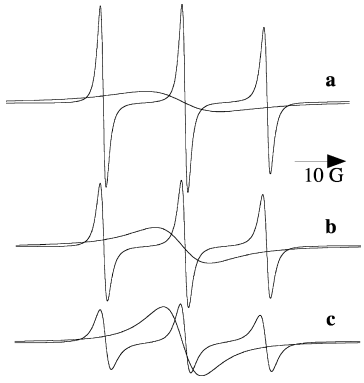

Figure 2. Least-squares fits to the monomer (narrow three-line) and micelle (broad single-line) spectra. Each of the four lines is the sum of an absorption and a dispersion component of Voigt shape.

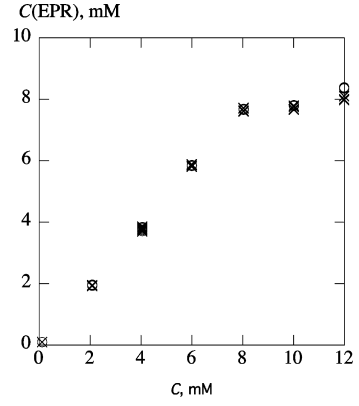

Figure 3. Concentration of the monomer spectrum estimated from the doubly integrated intensity of the narrow lines versus the total concentration at 298 K; $M_I = 0$ (○, individual values from 5 spectra) and $M_I = \pm 1$ (×, 2 values from each of 5 spectra). The cmc is observed at 8 mM where the intensities of the monomer lines level.

clearly observable as the point where the monomer concentration levels. This break point is constant with temperature within experimental uncertainty; thus, the cmc determined from these data are somewhat smaller than those published by Fox.[11] Only data in the range $c < 8$ mM are used in the rest of the present paper; however, it is interesting that employing data up to 12 mM, fitting just the narrow lines does not affect the results presented in Figures 4−9. In fact, fitting the narrow spectrum

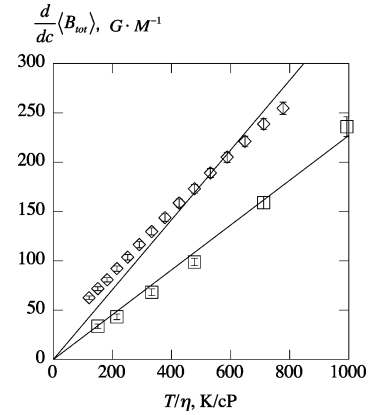

Figure 4. Total broadening constant versus T/η in water for DCAT12 (□) and PDT (◇).[7] The straight lines are least-squares fits with slopes 0.24 ($r = 0.998$) and 0.30 (G·cP)/(M·K) ($r = 0.999$), for DCAT12 and PDT, respectively (coefficients of correlation given in parentheses). Error bars are the probable errors in fitting the broadening to a linear function of the concentration plus 2% error in the concentration of PDT and DCAT12.

and ignoring the micelle spectrum yields reasonable results up to approximately 14 mM at $T > 313$ K. Above this concentration, the fitting of the center narrow line begins to be affected by the presence of the micelle line; however, the outside lines continue to give results near those that properly include the micelle line. Below 283 K, the micelle line becomes so broad that it does not appear in the residuals of narrow-line only fitting.

Values of $\langle B_{tot}\rangle$ vary linearly with c at all temperatures with coefficients of correlation larger than 0.999. For a typical plot of $\langle B_{tot}\rangle$ versus c, see, for example, Figure 4 of ref 7. In contemplating the challenge of studying DCAT12 as opposed to nonsurfactant nitroxides, it is useful to note that the maximum broadening observed in the present work is approximately 0.25 G compared with, for example, 5 G observed in ref 7. Line widths in the absence of spin−spin broadening are in the range 0.86−1.16 G.

Figure 4 shows values of the total broadening constant, $d\langle B_{tot}\rangle/dc$, as a function of T/η. Data for PDT taken from ref 7 are included and also in Figures 6−9 for comparison. The straight lines are least-squares fits constrained to the origin with slopes 0.30 and 0.24 (G·cP)/(M·K), for PDT and DCAT12, respectively. Although $d\langle B_{tot}\rangle/dc$ for DCAT12 is fit satisfactorily by a straight line, a slight curvature concave upward is apparent.

Figure 5 shows representative plots of averages of $\pm[V_{disp}/V_{pp}]^{\#}_{\pm}$ vs $\langle B_{tot}/A_0\rangle$ at 298 K (triangles, $r = 0.991$) and 353 K (squares, $r = 0.999$). For clarity, the ordinate of the 298 K data is displaced by +0.025. The straight lines are linear fits with coefficients of correlation indicated in the parentheses. Individual results from 5 spectra are plotted to show the reproducibility; the differences in $+[V_{disp}/V_{pp}]^{\#}_{+}$ and $-[V_{disp}/V_{pp}]^{\#}_{-}$ are smaller than the plot symbols.

The slopes of the linear least-squares fit lines in Figure 5 yield the percentage broadening by exchange, $\Omega(T)$, which are presented vs T/η in Figure 6a and vs τ_{rot}^{-1} in Figure 6b. Data for PDT in water (diamonds) and PDT in 70 wt % glycerol (circles) taken from the literature are included.[7] Figure 6a shows significant differences between the neutral PDT in the two solvents and the singly charged surfactant DCAT12 in water; however, these differences are smaller when viewed as functions of the rotational correlation rate, Figure 6b.

The broadening constant by spin exchange, $d\langle B_e\rangle/dc$, as a function of T/η is shown in Figure 7. The solid straight line is a least-squares fit with slope 0.35 ± 0.01 (G·cP)/(M·K) ($r =$

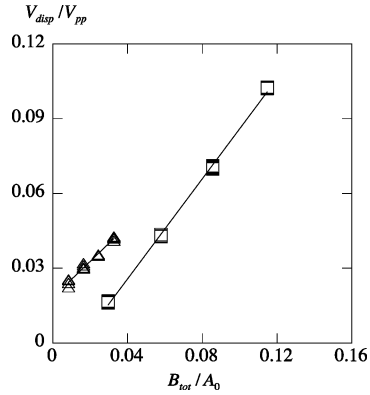

Figure 5. Dispersion versus total normalized broadening for DCAT12 in water at 298 K (△), ordinate displaced by 0.025 for clarity (r = 0.991) and 353 K (□) (r = 0.999) (coefficients of correlation indicated in parentheses). Five average values of $\pm[V_{disp}/V_{pp}]^{\#}_{\pm}$ (denoted by V_{disp}/V_{pp}) from five spectra taken one after the other on the same sample are plotted to show the reproducibility. The straight lines are linear fits. The slopes of the linear least-squares fit lines yield the percentage broadening by exchange. The differences in the results from $\pm[V_{disp}/V_{pp}]^{\#}_{\pm}$ are smaller than the plot symbols.

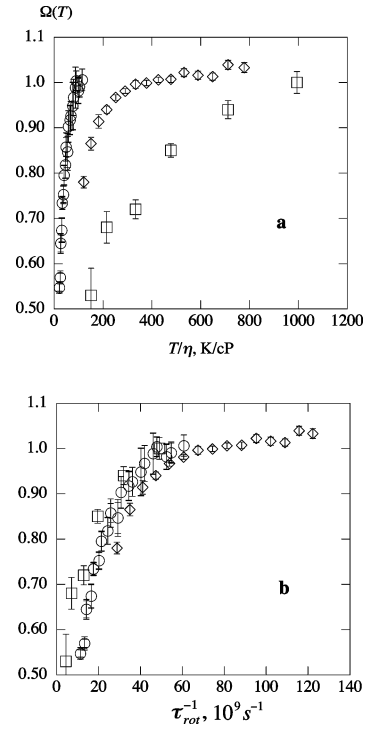

Figure 6. Fractional broadening by spin exchange in water versus (a) T/η and (b) rotational rate: DCAT12 (□) and PDT (◇).[7] Error bars are the estimated uncertainty in selecting the linear portion of curves like those in Figure 5. Data for PDT in 70 wt % glycerol[7] are included for comparison (○).

0.986) for PDT. The solid line through the DCAT12 data is a quadratic constrained to the origin as follows: $d\langle B_e\rangle/dc = (0.114 \pm 0.006)T/\eta + (1.26 \pm 0.009) \times 10^{-4} (T/\eta)^2$, r = 0.999 in G/M with T/η in K/cP. The error bars are propagated from the errors in $\Omega(T)$ and the total broadening constant. The dashed line is the Stokes−Einstein prediction for PDT, eq 12 with $r_{ex} = a$. The dotted line is the HD limit prediction for DCAT12 showing a remarkable agreement with the experimental data.

The dipolar broadening constant, $d\langle B_{dip}\rangle/dc$, is given vs η/T in Figure 8a and vs τ_{rot} in Figure 8b. The Stokes−Einstein prediction for PDT, eq 13, is shown as the dashed line in Figure 8a. Data for PDT in 70 wt % glycerol taken from the literature[7]

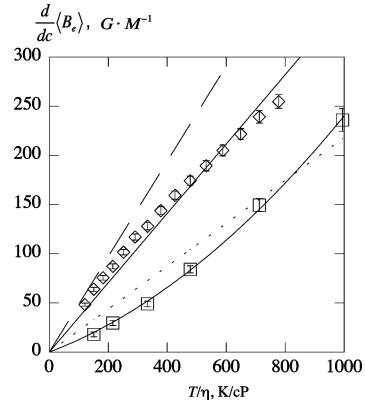

Figure 7. Exchange broadening constant in water versus T/η: DCAT12 (□) and PDT (◇).[7] The solid straight line is the least-squares fit to the PDT data with slope 0.35 ± 0.01 (G·cP)/(M·K) (r = 0.986). The solid line through the DCAT12 data is a quadratic constrained to the origin as follows: $d\langle B_e\rangle/dc = (0.114 \pm 0.006)T/\eta + (1.26 \pm 0.009) \times 10^{-4}(T/\eta)^2$, r = 0.999 in G/M with T/η in K/cP. The error bars are propagated from the errors in $\Omega(T)$ and the total broadening constant. The dashed line is the Stokes−Einstein prediction, eq 12, with $r_{ex} = a$ and the dotted line, the HD limit for DCAT12 with $f_e^* = 0.45$. The lines have no adjustable parameters.

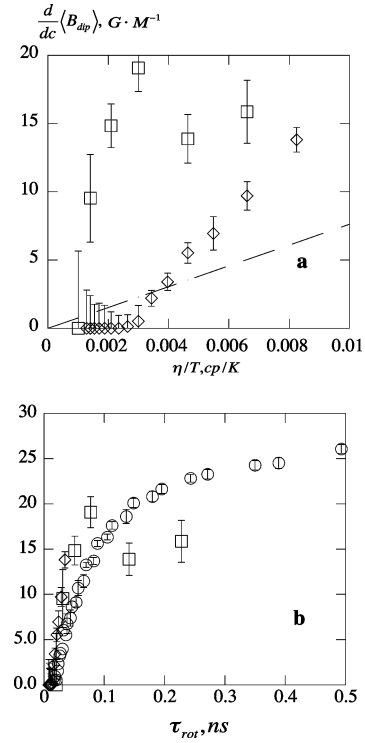

Figure 8. Dipolar broadening constant in water versus (a) η/T and (b) rotational rate: DCAT12 (□) and PDT (◇).[7] The dashed line is the Stokes−Einstein prediction for PDT. Error bars are propagated from the errors in $\Omega(T)$ and the total broadening constant. Data for PDT in 70 wt % glycerol[7] (○) are included in (b); these data are off scale in (a).

are off scale in Figure 8a but are included in Figure 8b. Note that there is a dramatic difference in the ranges of the abscissae of Figure 8a,b. The dipolar broadening constant for DCAT12 appears to reach a plateau of approximately 16 ± 3 G/M in water at approximately 283 ± 10 K. A similar plateau of 25 ± 1 G/M is observed for PDT in 70 wt % glycerol at approximately 273 K, however, at a value of η/T that is 30−50 times higher.[7] The difference in the rotational mobilities of the two nitroxides corresponding to these two plateaus is about a factor of 4. It is clear that the SE prediction for dipolar

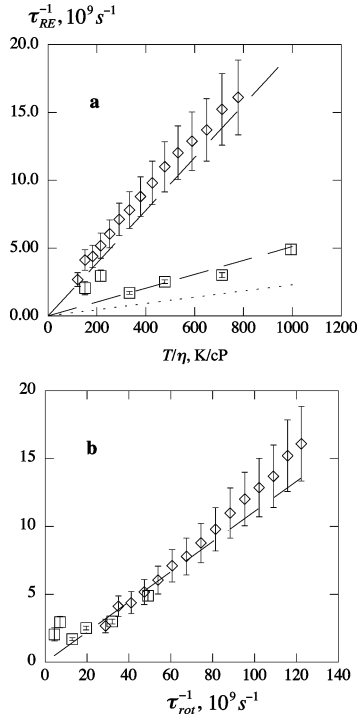

Figure 9. Re-encounter frequency in water versus (a) η/T and (b) rotational rate: DCAT12 (□) and PDT (◇). The dashed lines in (a) are eq 14 setting $b = 2a$ with a fixed by fitting eq 15 to rotational data yielding $a = 2.67$ Å for PDT and $a = 4.17$ Å for DCAT12. The dotted line in (a) is the HD limit for DCAT12 assuming $f^*_{RE} = f^*_{\bar{e}}$. In (b), the dashed line is eq 16. The lines in (a) and (b) have no adjustable parameters.

broadening can only be useful very near the origin (high values of T) of Figure 8 where, unfortunately, the data are subject to large errors. When Ω approaches unity, the calculation of $\langle B_{dip}\rangle$ becomes the small difference in the two large quantities $\langle B_e\rangle$ and $\langle B_{tot}\rangle$, eq 11. Furthermore, the computation of $\langle B_e\rangle$ from the dispersion is subject to larger errors at high values, leading to systematic errors that yield values of Ω slightly larger than unity, as is evident in Figure 6. These produce negative values of $\langle B_{dip}\rangle$, a nonphysical result. We hope to improve our determination of Ω when it approaches unity; however, in the meantime, the best we can do is to compare the initial slopes of the experimental data in Figure 8a with the SE prediction of C_{dip}/f^*_{dip}. This results in $f^*_{dip} = 1.0 \pm 0.3$ for PDT in 70 wt % glycerol, 0.3 ± 0.02 for PDT in water, and 0.07 ± 0.01 for DCAT12 in water. Thus, there is an order of magnitude reduction in the value of f^*_{dip} (an order of magnitude increase in the dipolar broadening constant) for the charged DCAT12. How much of that is due to the charge and how much is due to other factors, for example the attractive hydrophobic forces expected from a surfactant, is not yet known.

Plots of A_{abs}/A_0 vs $\langle B_e/A_0\rangle$ (not shown; see, for example, Figure 10 of ref 5) were fit to eq 17 and values of the re-encounter time, τ_{RE}, were computed using eq 18. The re-encounter rate is plotted as a function of T/η in Figure 9a and of τ_{rot}^{-1} in Figure 9b. The dashed lines in Figure 9a are eq 14, assuming that $b = 2a$ where the hydrodynamic radii are determined as follows: a plot of $\tau_{rot}{}^{-1}$ (Table 3) versus T/η is linear ($r = 0.998$) with slope $(0.0528 \pm 0.0015) \times 10^9$ (s·cP)/K. From eq 15, we compute $a = 4.17$ Å for DCAT12. Using data from ref 7, the same procedure produces $a = 2.67$ Å for PDT. The dotted line is the HD limit prediction for DCAT12 assuming that $f^*_{RE} = f^*_{\bar{e}} = 0.45$. Note that this hydrodynamic radius for PDT is considerably smaller than $a = 3.5$ Å computed from the method of Bondi and used in Figure 4 of ref 8. The dashed line in Figure 9b is a plot of eq 16 that shows remarkable consistency with the experimental data except for DCAT12 at 273 and 283 K. The dashed lines in Figure 9a,b are essentially the same content; however, in 9a the rotational data are smoothed by fitting to eq 15, while in Figure 9b they retain their individual measured values.

Discussion

Our expectation was that the broadening constants due to spin exchange $d\langle B_e\rangle/dc$ would be reduced due to coulomb repulsion, and Figure 7 shows this to be so. The dashed line is the SE prediction for an uncharged molecule, eq 12 with $a = r_{ex}$, and the dotted line is the HD limit for singly charged molecules. The nearly quantitative agreement between the HD limit and the experimental results for DCAT12 shows that strong exchange very likely prevails. Equation 12 shows remarkable agreement with PDT in a series of alkanes,[8] a series of aromatics,[26] as well as in water, Figure 7;[7] however, none of the experimental curves of $d\langle B_e\rangle/dc$ vs T/η is strictly linear. Note that the hydrodyamic radius does not come into the theory.

From values of f^*_{dip}, we find that the initial increase of $d\langle B_{dip}\rangle/dc$ is 14 ± 2 times faster than the hydrodynamic prediction for DCAT12 in water. For PDT, the initial increase is 3.3 ± 0.2 times faster in water and 1.0 ± 0.8 in 70% glycerol. The result in Figure 8b, where PDT in two solvents and DCAT12 in water show similar increases when plotted versus τ_{rot}, is very interesting. That the results for PDT in two solvents would form a common curve makes sense because the hydrodynamic radius is the same. However, that DCAT12 would also form a common curve is unanticipated. Note that the circles in Figure 8b representing data for PDT in 70% glycerol are completely off scale in Figure 8a where they ought to be compared with the dashed line. We resist making too much of this result until more data become available. Note that the very interesting effects of dipolar interaction on line spacing and the dispersion predicted by Galeev et al.[27] are not observed in the present work because the low values of T/η where these effects may be manifest, were avoided.

In Figure 9, the dashed lines are the hydrodynamic predictions of $\tau_{RE}{}^{-1}$, using the rotational motion to fix the hydrodynamic radii of PDT and DCAT12, respectively ignoring the charge of DCAT12. The dotted line represents the dilute limit of the expected rate for the charged DCAT12 employing $f^*_{RE} = f^*_{\bar{e}} = 0.45$. Unexpectedly, DCAT12 shows a re-encounter rate near that expected if it were not charged. Figure 9b, showing that the universal prediction eq 16 holds rather well for these two nitroxides, is a consequence of the good agreement of the experimental data with the SE result in Figure 9a. Equation 16 might not be expected to hold for DCAT12 for another reason: the value of hydrodynamic radius derived from rotational diffusion is expected to be less than that derived from translational diffusion because DCAT12 is a flexible probe.[28] One observes, for example, that the hydrodynamic radii of a series of doxyl labeled stearic acid methyl esters determined from τ_{rot} depend on the point of attachment of the nitroxide moiety while their geometric radii are the same.[28] Using a more realistic hydrodynamic radius for translation would reduce the theoretical prediction even more; i.e., the results would be even further from the theory. Finally, we've remarked that f^*_{RE} could be less than $f^*_{\bar{e}}$, which would reduce the theoretical prediction even further. Therefore, we cannot assume general validity of eq 16 on the basis of these limited results; nevertheless, if we are able to gain confidence in its generality from further work, a tremendous practical benefit will accrue because a measurement

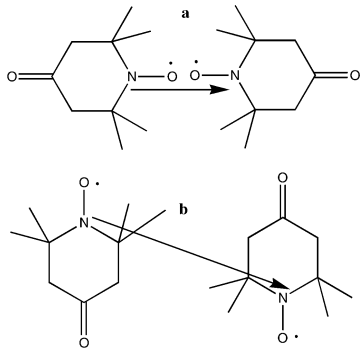

Figure 10. Rotation of each of the two nitroxides through $\pi/4$ radians effectively producing translation of the two unpaired electrons. The vectors connecting the two unpaired electrons are indicated. The magnitude of the translation scales with the size of the probe.

of τ_{rot} could be used to fix τ_{RE}^{-1}. Then, the line shifts could be used to provide an independent measurement of ω_e that could be used to verify values derived from the dispersion. Therefore, the re-encounter rate for DCAT12 is higher than expected and we cannot think of a simple explanation except that while two nitroxides are in close proximity, translation of the unpaired electron localized on the 2p orbital on nitrogen is strongly coupled to the rotation motion. Are we perhaps measuring re-encounters with a contribution from rotational motion which may not be strongly affected by coulomb repulsion? The basic idea is shown in Figure 10, which shows that a rotation of two PDT molecules by $\pi/2$ produces an effective translation of the unpaired electrons. An even larger effect would be expected for a larger molecule like DCAT12. Perhaps the curious result in Figure 8b may be understood partially by the mechanism of Figure 10.

One other point is worth mentioning. The simplified SE equation, used to derive eqs 12−14, is written using so-called stick boundary conditions for a spherical particle.[29] The same is true for the Stokes−Einstein−Debye equation leading to eq 15. Many authors have considered modifications to account for different boundary conditions and nonspherical shapes for both rotation and translation; see, for example ref 29 and references therein. Therefore, one expects systematic errors to arise in eqs 12−14 (translation) on the one hand and eq 15 (rotation) on the other. Assuming that these errors would be similar for rotation and translation, then determining a from τ_{rot} and using it in the Stokes−Einstein equation is expected to compensate for the errors somewhat. Kovarski et al.[30] showed that this approach is sound in rather complex fluid systems. The idea of combining translational and rotational hydrodynamic equations has been used, for example, by Tarjus and Kivelson[31] as the basis of their eq 3.

The net result of decreasing $d\langle B_e\rangle/dc$ and increasing $d\langle B_{dip}\rangle/dc$ for DCAT12 relative to PDT is to reduce rather dramatically the total broadening constant as shown in Figure 6a. This means that we must be careful not to assume that spin exchange dominates for charged nitroxides even in water at room temperature, where the percentage broadening by exchange is less than 75%. The intriguing correlation of values of Ω between PDT in two solvents and DCAT12 when plotted versus the rotational rate cannot be predicted from hydrodynamic theory.

It is useful to keep in mind that the dipolar broadening is rather small, reaching a maximum of 0.23 G for 8 mM DCAT12 at 273 K. Future studies of charged (nonsurfactant) nitroxides will provide a wider range of data because one will not be limited to a maximum concentration of $c <$ cmc.

Conclusions

In water, compared with the uncharged PDT, the singly charged surfactant DCAT12 shows (1) decreased values of $d\langle B_e\rangle/dc$, (2) increased values of $d\langle B_{dip}\rangle/dc$, and (3) decreased values of τ_{RE}^{-1}. Item (1) is remarkably well predicted by the HD limit of the SE equation, eq 12. Item (3) is well predicted by the SE result, eq 14, using the hydrodynamic radius estimated from the rotational correlation time, however, only if we ignore the charge. The SE prediction for $d\langle B_{dip}\rangle/dc$ is reasonably accurate only for PDT in 70 wt % glycerol near the origin. For PDT and DCAT12 in water, the increase of $d\langle B_{dip}\rangle/dc$ with η/T is more rapid than the hydrodynamic prediction. Values of Ω and $d\langle B_{dip}\rangle/dc$ for PDT in water and 70 wt % glycerol, as well as DCAT12 in water form approximately common curves when plotted against τ_{rot}^{-1} or τ_{rot}, respectively, results that cannot be predicted by hydrodynamic theory.

Acknowledgment. We gratefully acknowledge support from NIH grant 2 S06 GM048680.

References and Notes

(1) Molin, Y. N.; Salikhov, K. M.; Zamaraev, K. I. *Spin Exchange. Principles and Applications in Chemistry and Biology*; Springer-Verlag: New York, 1980; Vol. 8.
(2) Salikhov, K. M. *J. Magn. Reson.* **1985**, *63*, 271.
(3) Bales, B. L.; Peric, M. *J. Phys. Chem. B* **1997**, *101*, 8707.
(4) Bales, B. L.; Peric, M. *J. Phys. Chem. A* **2002**, *106*, 4846.
(5) Bales, B. L.; Peric, M.; Dragutan, I. *J. Phys. Chem. A* **2003**, *107*, 9086.
(6) Bales, B. L.; Meyer, M.; Smith, S.; Peric, M. *J. Phys. Chem A* **2008**, *112*, 2177.
(7) Bales, B. L.; Meyer, M.; Smith, S.; Peric, M. *J. Phys. Chem A* **2009**, *113*, 4930.
(8) Kurban, M. R.; Peric, M.; Bales, B. L. *J. Chem. Phys.* **2008**, *129*, 064501.
(9) Debye, P. *Trans. Electrochem. Soc.* **1942**, *82*, 265.
(10) Fox, K. K. *Trans. Faraday Soc.* **1971**, *67*, 2802.
(11) Fox, K. K. *J. Chem. Soc., Faraday Trans. 1* **1978**, *74*, 220.
(12) Coughlin, R. T.; Caldwell, C. R.; Haug, A.; McGroarty, E. J. *Biochem. Biophys. Res. Commun.* **1981**, *100*, 1137.
(13) Quintanilha, A. T.; Packer, L. *Arch. Biochem. Biophys.* **1978**, *190*, 206.
(14) Cafiso, D.; Hubbell, W. L.; Quintanilha, A. T. *Methods Enzymol.* **1982**, *88*, 682.
(15) Hashimoto, K.; Angiolillo, P.; Rottenberg, H. *Biochim. Biophys. Acta* **1984**, *764*, 55.
(16) Tikhonov, A. N.; Khomutov, G. B.; Ruuge, E. K.; Blumenfeld, L. A. *Biochim. Biophys. Acta* **1981**, *637*, 321.
(17) Martini, G.; Bindi, M. *J. Colloid Interface Sci.* **1985**, *108*, 133.
(18) Eastman, M. P.; Bruno, G. V.; Freed, J. H. *J. Chem. Phys.* **1970**, *52*, 2511.
(19) Eigen, M. *Z. Phys. Chem.* **1954**, *1*, 176.
(20) Keith, A. D.; Snipes, W.; Mehlhorn, R. J.; Gunter, T. *Biophys. J.* **1977**, *19*, 205.
(21) Bales, B. L. Inhomogeneously Broadened Spin-Label Spectra. In *Biological Magnetic Resonance*; Berliner, L. J. L. J., Reuben, J., Eds.; Plenum Publishing Corp.: New York, 1989; Vol. 8, pp 77.
(22) Berner, B.; Kivelson, D. *J. Phys. Chem.* **1979**, *83*, 1406.
(23) Levine, I. N. *Physical Chemistry*, 4th ed.; McGraw-Hill: New York, 1995.
(24) Smoluchowski, M. V. *Z. Phys. Chem.* **1917**, *92*, 129.
(25) Jones, L. L.; Schwartz, R. N. *Mol. Phys.* **1981**, *43*, 527.
(26) Kurban, M. R. *J. Chem. Phys.* **2009**, *130*, 104502.
(27) Galeev, R. T.; Salikhov, K. M. *Chem. Phys. Rep.* **1996**, *15*, 359.
(28) Lebedeva, N. V.; Bales, B. L. *J. Phys. Chem. B* **2006**, *110*, 9791.
(29) Dote, J.; Kivelson, D.; Schwartz, R. N. *J. Phys. Chem.* **1981**, *85*, 2169.
(30) Kovarskii, A. L.; Wasserman, A. M.; Buchachenko, A. L. *J. Magn. Reson.* **1972**, *7*, 225.
(31) Tarjus, G.; Kivelson, D. *J. Chem. Phys.* **1995**, *103*, 3071.
(32) Bales, B. L.; Stenland, C. *J. Phys. Chem.* **1993**, *97*, 3418.
(33) Bales, B. L.; Peric, M.; Lamy-Freund, M. T. *J. Magn. Reson.* **1998**, *132*, 279.

JP905335R